ESR Spectra of Benzene Anion

Minoru KIMURA,† Hiroyuki KAWABE, Kiyoshi NISHIKAWA, and Shigeyuki AONO*
†*Department of Physics, Faculty of Science, Kanazawa University, Marunouchi, Kanazawa 920*
Department of Chemistry, Faculty of Science, Kanazawa University, Marunouchi, Kanazawa 920
(Received April 27, 1985)

Based on the spin density calculated in our previous paper,[1] the ESR spectra of the benzene anion (exactly the dihydrophenylide ion) are analyzed by the Bloch equation. A hyperfine spectrum broader than those of usual aromatic radicals attributes to the chemical exchange process that the ion in question surrounded by solvent molecules undergoes a rotational motion characterized by the time τ which is the life time of chemical exchange. The line shape for each hyperfine spectrum is given in terms of $1/T_2$ and τ under the condition of $\tau/T_2 \ll 1$.

It is an old story that, in the liquid state, the ESR spectra of the benzene anion were considerably broader[2] than those of usual aromatic radicals with less symmetric character as naphthalene anion (dihydronaphthylide ion). The similar phenomena have been observed in coronene and triphenylene,[2] which suggest that the unusual broad lines may be associated with the Jahn-Teller distortion. The normal states of those ions would be orbitally degenerate if the original symmetries of the parent molecules were retained. If the vibronic interaction is introduced to this system, the orbital degeneracy will be removed and the lattice distortion should arise (the Jahn-Teller effect). McConnell and McLachlan[3] have studied this in such a way that the electronic part is based on the Hückel approximation and the vibronic part is considerably elaborated. In our previous paper,[1] we have investigated the same problem by the Hubbard Hamiltonian with the vibronic interaction (including the dominant part of electron correlation). Both results agree with each other in the limitting case of the electron correlation being negligible. However, the latter demonstrates the important effect of the electron correlation which causes the negative spin densities at opposing corners of the benzene anion. In the second half of their paper,[3] McConnell and McLachlan discussed about the broad lines from the view points of chemical exchange briefly and only qualitatively. The main purpose of the present paper is to analyze the line shape in more detail, using the Bloch equation with chemical exchange.

A deutrium substitution of a hydrogen has been used in order to lift experimentally the orbital degeneracy. In this way, the complicated but sometimes well resolved spectra have been observed not only for the benzene anion[4] but also for more complicated radicals.[5] We consider that these observations partly support the chemical exchange mechanism with the reduction of symmetry due to the Jahn-Teller distortion for the unusual broad line.

Line Shape Analysis of Bloch Equation with Chemical Exchange

Let us consider the Bloch equation for some conformation X which appears during the chemical exchange process,[6]

$$\frac{dG_X}{dt} + \eta_X G_X = -i\omega_1 M_0, \tag{1}$$

where

$$G_X = u_X + iv_X,$$
$$\eta_X = \frac{1}{T_2} - i(\Delta\omega + \omega_X), \tag{2}$$

and u and v are the in-phase and out-of-phase magnetization. The latter being responsible for the absorption process, we are interested in the imaginary part of G. And $\omega_1 = \gamma_e H_1$, γ_e is the gyromagnetic ratio of electron, H_1 is the magnitude of the applied microwave field, assuming no saturation, $M_0 \approx M_z$, M_z is the static magnetization along the direction of the external field, T_2 is the transverse relaxation time without taking into account of chemical exchange, ω_X is the hyperfine shift due to proton, $\Delta\omega = \omega_0 - \omega$ with $\omega_0 = \gamma_e H_0$, H_0 is the intensity of the external field along the z-axis and ω is the frequency.

Equation 1 gives the result,

$$G_X(t) = -\frac{i\omega_1 M_0}{\eta_X}\{1 - \exp(-\eta_X t)\} + G_X^0 \exp(-\eta_X t), \tag{3}$$

where

$$G_X^0 = G_X(t=0). \tag{4}$$

Assuming the characteristic time τ_X for the conformation X, we have the time average of $G_X(t)$ as,

$$\bar{G}_X = \frac{1}{\tau_X}\int_0^\infty G_X(t) \exp(-t/\tau_X) dt$$
$$= -\frac{i\omega_1 M_0}{1+\eta_X\tau_X} + \frac{G_X^0}{1+\eta_X\tau_X}. \tag{5}$$

In order to relate $\bar{G}_X$ with the observation we have to average over all possible values of G_X^0. The value of G_X^0 depends on the immediate past of the system. If the molecular conformation changes to the conformation X from the conformations I's with the probabilities ρ_I's, it follows that

$$\langle G_X^0 \rangle = \sum_I{}' \rho_I \langle \bar{G}_I \rangle, \tag{6}$$

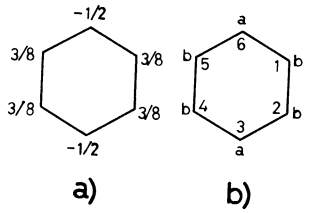

Fig. 1. Spin distribution in the benzene anion. a): Strong correlation limit, b): General case. The numbers indicate the site.

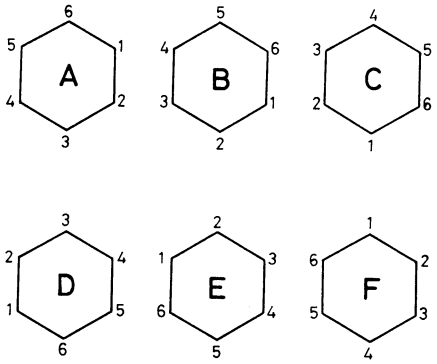

Fig. 2. Various orientations of the benzene anion. The conformations *A*—*F* appear with the rotational motion of anion. The numbers indicate the sites and the spin densities are *a* at the sites 3 and 6, and *b* at the other sites.

but the summation with a prime is restricted to the immediate past conformations for X. From Eqs. 5 and 6 we get the following relation,

$$\langle\bar{G}_X\rangle = -\frac{i\omega_1 M_0}{1+\eta_X\tau_X} + \frac{1}{1+\eta_X\tau_X}\sum_I{}'\rho_I\langle\bar{G}_I\rangle. \tag{7}$$

This procedure of incorporating the second term corresponds to including chemical exchange. The actual observation can be interpreted from

$$\langle G\rangle = \sum_X P_X\langle\bar{G}_X\rangle, \tag{8}$$

where P_x is the existing probability of conformation X and the summation is over the all possible conformations.

Physical Model

In our previous paper,[1] we obtained for the benzene anion the state in which the spin distribution is shown in Fig. 1a (the strong correlation limit) and in Fig.1b (general case). As was stressed there, these are the cases that the anion is fixed for a characteristic time τ by the solvent effect. We assume that the anion rotates from time to time to take various orientations as shown in Fig. 2 and each conformation has the same characteristic time τ and the same probability of existance, namely, $P_x=1/6$.

Look at the conformation A in Fig. 2. The immediate past history of this conformation should be either B or F, each of which changes into A with the same probability 1/2. Therefore. Eq. 7 becomes

$$\langle\bar{G}_A\rangle = -\frac{i\omega_1 M_0\tau}{1+\eta_A\tau} + \frac{\langle\bar{G}_B\rangle+\langle\bar{G}_F\rangle}{2(1+\eta_A\tau)}, \tag{9}$$

which is abbreviated as

$$g_A + c_A(g_B+g_F) = d_A \tag{10}$$

where

$$g_A = \langle\bar{G}_A\rangle,$$
$$c_A = -\frac{1}{2(1+\eta_A\tau)},$$
$$d_A = -\frac{i\omega_1 M_0\tau}{1+\eta_A\tau}. \tag{11}$$

For the other conformations similar equations hold. They are altogether written in matrix form as

$$\begin{bmatrix} g_A \\ g_B \\ g_C \\ g_D \\ g_E \\ g_F \end{bmatrix} = \begin{bmatrix} 1 & c_A & 0 & 0 & 0 & c_A \\ c_B & 1 & c_B & 0 & 0 & 0 \\ 0 & c_C & 1 & c_C & 0 & 0 \\ 0 & 0 & c_D & 1 & c_D & 0 \\ 0 & 0 & 0 & c_E & 1 & c_E \\ c_F & 0 & 0 & 0 & c_F & 1 \end{bmatrix}^{-1} \begin{bmatrix} d_A \\ d_B \\ d_C \\ d_D \\ d_E \\ d_F \end{bmatrix}, \tag{12}$$

and $\langle G\rangle$ related to the actual observation can be obtained by

$$\langle G\rangle = \frac{1}{6}\sum_X g_X. \tag{13}$$

From Eqs. 12 and 13 we obtain

$$\langle G\rangle = \frac{1}{6}\frac{1}{\det}\sum_X d_X F_X, \tag{14}$$

where

$$\det = \begin{vmatrix} 1 & c_A & 0 & 0 & 0 & c_A \\ c_B & 1 & c_B & 0 & 0 & 0 \\ 0 & c_C & 1 & c_C & 0 & 0 \\ 0 & 0 & c_D & 1 & c_D & 0 \\ 0 & 0 & 0 & c_E & 1 & c_E \\ c_F & 0 & 0 & 0 & c_F & 1 \end{vmatrix},$$
$$F_A = 1 - c_B - c_F - c_Cc_D - c_Dc_E + c_B(c_Dc_E+c_Ec_F) + c_F(c_Bc_C+c_Cc_D) + c_Bc_Cc_Dc_E - c_Ec_F(c_Bc_C-c_Cc_D) - 2c_Bc_Cc_Dc_Ec_F. \tag{15}$$

In obtaining F_B—F_F, we need only the cyclic permutation of suffixes in the second formula in Eq. 15, step by step.

Now we turn to evaluate the hyperfine shifts.

(1) I_Z=3: Every protons have the up spin.

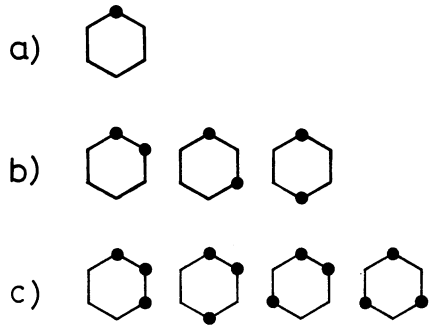

Fig. 3. Irreducible patterns. The solid circles indicate the sites to which the protons with down spin link.
a): For $I_z=2$, b): For $I_z=1$, c): For $I_z=0$.

In this case, every conformations designated by A—F in Fig. 2 have the same proton hyperfine shift. *i.e.*,

$$\omega_A = \omega_B = \omega_C = \omega_D = \omega_E = \omega_F = 2a + 4b \quad [1],$$

where we omit the multiplicative constant, Q ($\approx$23 G, 1 G=10^{-4} T), for simplicity, a is the spin density at the sites 3 and 6, b at the other sites and the number in the square bracket indicates the degeneracy number.

(2) $I_Z=2$: One of the six protons has the down spin.

This case is displayed by the irreducible pattern shown in Fig. 3a. Combining this with the patterns shown in Fig. 2, we obtain

$$\omega_A = \omega_D = 4b,$$
$$\omega_B = \omega_C = \omega_E = \omega_F = 2a + 2b \quad [6].$$

(3) $I_Z=1$: Two of the six protons have the down spin.

This case is classified into three subcases as displayed by the irreducible patterns shown in Fig. 3b. The hyperfine shift will be calculated for each,

$$\text{(3a)}\quad \omega_A = \omega_B = \omega_D = \omega_E = 2b,$$
$$\omega_C = \omega_F = 2a \quad [6],$$
$$\text{(3b)}\quad \omega_A = \omega_C = \omega_D = \omega_F = 2b,$$
$$\omega_B = \omega_E = 2a \quad [6].$$
$$\text{(3c)}\quad \omega_B = \omega_C = \omega_E = \omega_F = 2a,$$
$$\omega_A = \omega_D = -2a + 2b \quad [6].$$

(4) $I_Z=0$: A half of the six protons have the down spin.

This case has four subcases which are displayed in Fig. 3c. The hyperfine shift is expressed as follows

$$\text{(4a)}\quad \omega_A = \omega_B = \omega_C = \omega_D = \omega_E = \omega_F = 0 \quad [6],$$
$$\text{(4b)}\quad \omega_A = \omega_D = -2a + 2b,$$
$$\omega_B = \omega_E = 0,$$
$$\omega_C = \omega_F = 2a - 2b \quad [6],$$
$$\text{(4c)}\quad \omega_A = \omega_D = 0,$$
$$\omega_B = \omega_E = -2a + 2b,$$
$$\omega_C = \omega_F = 2a - 2b \quad [6],$$
$$\text{(4d)}\quad \omega_A = \omega_B = \omega_C = \omega_D = \omega_E = \omega_F = 0 \quad [2].$$

Line Shape

In order to obtain the line shape for every hyperfine components, it is convenient to re-classify the above mentioned cases as follows.

Group 1: $\omega_A=\omega_B=\omega_C=\omega_D=\omega_E=\omega_F$.

This group consists of the three cases (1), (4a), and (4d). We calculate $\langle G\rangle$ by Eq. 14, and obtain

$$\langle G\rangle = \frac{d}{(1+2c)}, \tag{16}$$

where we used the relation

$$c = c_A = c_B = c_C = c_D = c_E = c_F,$$
$$d = d_A = d_B = d_C = d_D = d_E = d_F. \tag{17}$$

Substituting Eqs. 1 and 11 into Eq. 16, we have

$$\langle G\rangle = \frac{1}{(1/T_2)^2+(\Delta\omega+\omega_A)^2}\left\{-\omega_1 M_0 \Delta\omega + i\omega_1 M_0 \frac{1}{T_2}\right\}, \tag{18}$$

of which the imaginary part is

$$v = \frac{\omega_1 M_0/T_2}{(1/T_2)^2+(\Delta\omega+\omega_A)^2}. \tag{19}$$

Thus we get a Lorentzian line shape with the resonance frequency $\Delta\omega$, the peak height v_{peak} and the natural width $\Delta\omega_{1/2}$ given by

$$\Delta\omega = -\omega_A,$$
$$v_{peak} = \omega_1 M_0 T_2,$$
$$\Delta\omega_{1/2} = \frac{1}{T_2}. \tag{20}$$

Group 2: $\omega_A=\omega_D$, $\omega_B=\omega_C=\omega_E=\omega_F$.

This group consists of the two cases (2) and (3c). In the present case we have

$$\langle G\rangle = \frac{1}{6}\left\{\frac{2d_A(1-c_B)+4d_B(1-c_A)}{1-2c_Ac_B+c_B}\right\}. \tag{21}$$

Thus

$$v = \frac{-\omega_1 M_0\{1/T_2+4/27\cdot(\omega_A-\omega_B)^2\tau\}}{\{1/T_2-2/3\cdot(\Delta\omega+\omega_A)(\Delta\omega+\omega_B)\tau\}^2+\{\Delta\omega+1/3\cdot(\omega_A+2\omega_B)\}^2}. \tag{22}$$

In getting this result, we have assumed $\tau/T_2 \ll 1$, since $\tau\approx10^{-10}$ s[7] and for free radicals in solution the natural width of resonance lines is typically $\approx$0.1 G,[8] which is correspond to $T_2\approx10^{-6}$ s.

We proceed further by carrying out an approximate calculation. Obviously we have a resonance line around $\Delta\omega=-\omega_A$ where v takes the value given by

$$v_{\text{peak}} = -\omega_1 M_0 \left[\frac{1/T_2 + 4/27 \cdot (\omega_A - \omega_B)^2 \tau}{(1/T_2)^2 + 4/9 \cdot (\omega_A - \omega_B)^2} \right]. \quad (23)$$

Noting that $\omega_A - \omega_B \approx 10^7\ \text{s}^{-1}$, $\tau(\omega_A - \omega_B) \approx 10^{-3}$ and $\tau/T_2 \approx 10^{-4}$, we have $v_{\text{peak}} \fallingdotseq -\omega_1 M_0/(3/\tau)$. The corresponding half width being $3/\tau$, we add this to the natural width $1/T_2$ to obtain

$$v_{\text{peak}} = \frac{-\omega_1 M_0}{3/\tau + 1/T_2},$$
$$\Delta\omega_{1/2} = \frac{3}{\tau} + \frac{1}{T_2}. \quad (24)$$

In the same way, we obtain the corresponding expressions for another resonance at $\Delta\omega = -\omega_B$

$$v_{\text{peak}} = \frac{-\omega_1 M_0}{3/4\tau + 1/T_2},$$
$$\Delta\omega_{1/2} = \frac{3}{4\tau} + \frac{1}{T_2}. \quad (25)$$

and for the one at $\Delta\omega = -(\omega_A + 2\omega_B)/3$,

$$v_{\text{peak}} = \frac{-\omega_1 M_0}{4/27 \cdot (\omega_A - \omega_B)^2 \tau + 1/T_2},$$
$$\Delta\omega_{1/2} = \frac{4}{27}(\omega_A - \omega_B)^2 \tau + \frac{1}{T_2}. \quad (26)$$

Group 3: $\omega_B = \omega_E$, $\omega_A = \omega_C = \omega_D = \omega_F$.

This group consists of the single case (3b). Various lines belonging to this group can be described by interchanging suffixes A and B of Eqs. 24—26, that is,

$$\Delta\omega = -\omega_B,$$
$$v_{\text{peak}} = \frac{-\omega_1 M_0}{3/\tau + 1/T_2},$$
$$\Delta\omega_{1/2} = \frac{3}{\tau} + \frac{1}{T_2}, \quad (27)$$

and

$$\Delta\omega = -\omega_A,$$
$$v_{\text{peak}} = \frac{-\omega_1 M_0}{3/4\tau + 1/T_2},$$
$$\Delta\omega_{1/2} = \frac{3}{4\tau} + \frac{1}{T_2}, \quad (28)$$

and

$$\Delta\omega = -\frac{1}{3}(\omega_B + 2\omega_A),$$
$$v_{\text{peak}} = \frac{-\omega_1 M_0}{4/27 \cdot (\omega_B - \omega_A)^2 \tau + 1/T_2},$$
$$\Delta\omega_{1/2} = \frac{4}{27}(\omega_B - \omega_A)^2 \tau + \frac{1}{T_2}. \quad (29)$$

Group 4: $\omega_C = \omega_F$, $\omega_A = \omega_B = \omega_D = \omega_E$.

This group also consists of the single case (3a). In this case, replacing B in the equations obtained in Group 3 by C, we obtain

$$\Delta\omega = -\omega_C,$$
$$v_{\text{peak}} = \frac{-\omega_1 M_0}{3/\tau + 1/T_2},$$
$$\Delta\omega_{1/2} = \frac{3}{\tau} + \frac{1}{T_2}, \quad (30)$$

and

$$\Delta\omega = -\omega_A,$$
$$v_{\text{peak}} = \frac{-\omega_1 M_0}{3/4\tau + 1/T_2},$$
$$\Delta\omega_{1/2} = \frac{3}{4\tau} + \frac{1}{T_2}, \quad (31)$$

and

$$\Delta\omega = -\frac{1}{3}(\omega_C + 2\omega_A),$$
$$v_{\text{peak}} = \frac{-\omega_1 M_0}{4/27 \cdot (\omega_C - \omega_A)^2 \tau + 1/T_2},$$
$$\Delta\omega_{1/2} = \frac{4}{27}(\omega_C - \omega_A)^2 \tau + \frac{1}{T_2}. \quad (32)$$

Group 5: $\omega_A = \omega_D$, $\omega_B = \omega_E$, $\omega_C = \omega_F$.

This group consists of the two cases (4b) and (4c). In a similar way as used in the previous cases, we obtain

$$\langle G \rangle = \frac{1}{3} \frac{[d_A(1 - c_B - c_C + c_B c_C) + d_B(1 - c_C - c_A + c_C c_A) + d_C(1 - c_A - c_B + c_A c_B)]}{(1 - c_A c_B - c_B c_C - c_C c_A + 2c_A c_B c_C)}. \quad (33)$$

Thus

$$v = \frac{-\omega_1 M_0 [1/T_2 + 4\tau/9 \cdot W(\Delta\omega)]}{[1/T_2 + 4\tau/9 \cdot X^2(\Delta\omega)]^2 + 1/9 \cdot Y^2(\Delta\omega)}, \quad (34)$$

where

$$X^2(\Delta\omega) = \Delta_A\Delta_B + \Delta_B\Delta_C + \Delta_C\Delta_A,$$
$$Y(\Delta\omega) = \Delta_A + \Delta_B + \Delta_C, \quad (35)$$

with the abbreviations of, for example,

$$\Delta_A = \Delta\omega + \omega_A,$$
$$W(\Delta\omega) = X^2(\Delta\omega) - \frac{1}{3}Y^2(\Delta\omega)$$
$$= \Delta_A\Delta_B + \Delta_B\Delta_C + \Delta_C\Delta_A - \frac{1}{3}(\Delta_A + \Delta_B + \Delta_C)^2. \quad (36)$$

Resonance lines will appear at the frequencies obtained from $X^2(\Delta\omega) = 0$ and $Y^2(\Delta\omega) = 0$.

In the latter case, the situation is rather simple and we obtain

$$\Delta\omega = -\frac{1}{3}(\omega_A + \omega_B + \omega_C),$$
$$v_{\text{peak}} = \frac{-\omega_1 M_0}{1/T_2 + 4\tau/9 \cdot W(\Delta\omega)},$$

$$\Delta\omega_{1/2} = \frac{1}{T_2} + \frac{4\tau}{9}W(\Delta\omega). \quad (37)$$

In the former, we begin with solving $X^2(\Delta\omega)=0$ and obtain two solutions,

$$\begin{aligned}\Delta\omega &= \omega_+ \text{ and } \omega_- \\ &= -(\omega_A+\omega_B+\omega_C) \\ &\pm\sqrt{(\omega_A+\omega_B+\omega_C)^2-1/3\cdot(\omega_A\omega_B+\omega_B\omega_C+\omega_C\omega_A)}. \quad (38)\end{aligned}$$

At $\Delta\omega=\omega_+$ for example, we have

$$v_{peak} = \frac{-\omega_1 M_0[1/T_2+4\tau/9\cdot W(\omega_+)]}{(1/T_2)^2+1/9\cdot Y^2(\omega_+)}. \quad (39)$$

Employing the approximate procedure to obtain Eq. 24, we get

$$\begin{aligned}&\Delta\omega = \omega_k \quad (k \text{ is } + \text{ or } -.), \\ &v_{peak} = \frac{-\omega_1 M_0}{Y^2(\omega_k)/[4\tau W(\omega_k)]+1/T_2}, \\ &\Delta\omega_{1/2} = \frac{Y^2(\omega_k)}{4\tau W(\omega_k)} + \frac{1}{T_2}. \quad (40)\end{aligned}$$

We should like to emphasize that there are three kinds of lines from the view point of the τ dependence. The first one has the peak height which is independent of τ, as given in Eq. 20, the second one is given by Eqs. 26, 29, 32, and 37, roughly speaking, v_{peak} is inversely proportional to τ and the third one is given by Eqs. 24, 25, 27, 28, 30, 31, and 40, v_{peak} is inversely proportional to τ^{-1}, namely proportional to τ. Let us consider the usual (high temperature) case. Although the value of τ becomes smaller and smaller with increasing temperature, the line shape of the first one is temperature independent, while in the second one the line shape is determined mainly by $1/T_2$ and the third one disappears.

Numerical Analysis and Discussions

In order to help our understanding, we deal with the high temperature limit. *i.e.*, $\tau=0$. In this case, the resonance lines of which peak heights are independent of τ and are inversely proportional to τ will appear. From Eqs. 19 and 26 we can see $\Delta\omega=1/T_2$ and $v_{peak}=-\omega_1 M_0 T_2$ by putting $\tau=0$. Therefore, the peak heights are determined by the number of degeneracy. In Table 1 the groups in the previous section, the resonance frequencies and the degeneracy numbers are listed. Obviously the peak heights for each resonance line are described by the binomical coefficients and the resonance frequencies are equally spaced. Note that as seen from Fig. 1b 2a+4b is the total spin density. Therefore, in the high temperature limit the spaces are independent of the spin density distribution.

For various values of τ, we can simulate the line shapes as shown in Figs. 4 and 5. We can see how the

Table 1. The states of nuclear spin and hyperfine coupling constant

Group	I_z	$-\omega_R/Q$[a)]	D[a)]
1	3	$2a+4b$	1
	0	0	6
	0	0	2
2	2	$2/3(2a+4b)$	6
	2	$1/3(2a+4b)$	3
3	1	$1/3(2a+4b)$	6
4	1	$1/3(2a+4b)$	6
5	0	0	6
	0	0	6

a) ω_R is the resonance frequency, Q is the constant which relate the spin density to the hyperfine splitting, so ω_R/Q is the resonance frequency in Q unit and D is the number of degeneracy.

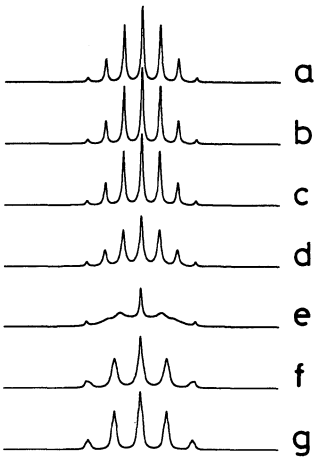

Fig. 4. Line shapes. $T_2=1.0\times10^{-6}$ s, $a=0.24$, $b=0.005$. a): $\tau=1.0\times10^{-12}$ s, b): $\tau=1.0\times10^{-11}$ s, c): $\tau=1.0\times10^{-10}$ s, d): $\tau=1.0\times10^{-9}$ s, e): $\tau=1.0\times10^{-8}$ s, f): $\tau=1.0\times10^{-7}$ s, g): $\tau=1.0\times10^{-6}$ s.

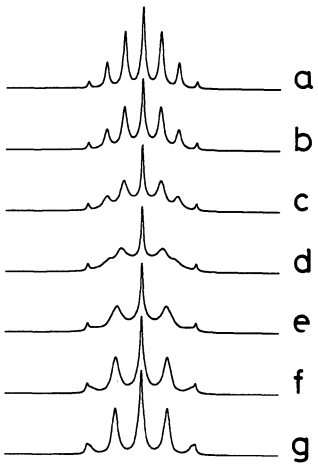

Fig. 5. The qualitative change of line shapes. $T_2=1.0\times10^{-6}$ s, $a=0.24$, $b=0.005$. a): $\tau=1.25\times10^{-9}$ s, b): $\tau=2.5\times10^{-9}$ s, c): $\tau=5.0\times10^{-9}$ s, d): $\tau=1.0\times10^{-8}$ s, e): $\tau=2.0\times10^{-8}$ s, f): $\tau=4.0\times10^{-8}$ s, g): $\tau=8.0\times10^{-8}$ s.

line shapes change as the values of τ are increased: The different behaviors of three type of lines as mentioned in the last part of the previous section are discernible. Under the condition of $\tau/T_2 \ll 1$ (the cases Figs. 4a—d), the lines whose intensities are proportional to τ hardly appear. This should correspond to the actual experiment.[2] The extremely narrow lines with $\tau=10^{-12}$ s in Fig. 4a are such ones as observed in the aromatic anions of the less symmetry, *e.g.*, naphthalene anion. The lines in Fig. 4c or Fig. 4d which correspond to $\tau=10^{-10}$ or 10^{-9} s, respectively, have considerable likeliness with the observed ones. We can guess that the benzene anion tumbles in this time scale in solution.

As τ gets larger, the lines which are neglected in the case of $\tau \fallingdotseq 0$ are seen. This makes the line structure complicated and results in the apparent broad lines as seen in Figs. 4e—g. Note that in computer simulation line shapes are directly described without the condition of $\tau/T_2 \ll 1$. From Figs. 4f and 4g, we can see patterns which are qualitatively different from Figs. 4a—e. The last three cases have not been observed in experiments yet. The transient patterns in this change are shown in Fig. 5. Here we can observe that the second line from the edge is gradually disappearing.

References

1) M. Kimura, H. Kawabe, K. Nishikawa, and S. Aono, *Bull. Chem. Soc. Jpn.*, **58**, 2756 (1985).

2) M. G. Townsent and S. I. Weissman, *J, Chem. Phys.*, **32**, 309 (1960).

3) H. M. McConnell and A. D. McLachlan, *J. Chem. Phys.*, **34**, 1 (1961).

4) R. G. Lawler, J. R. Bolton, G. K. Fraenkel, and T. H. Brown, *J. Am. Chem. Soc.*, **86**, 520 (1964).

5) K. Mukai, T. Mishima, and K. Ishizu, *J. Chem. Phys.*, **66**, 1680 (1977).

6) A. Carrington, *Mol. Phys.*, **5**, 425 (1962).

7) S. Aono and I. Ohno, *Kogyo. Kagaku. Zassi*, **68**, 1530 (1965).

8) J. E. Wertz and J. R. Bolton, "ELECTRON SPIN RESONANCE," McGraw-Hill, New York, (1972).